Estimation of the Wall Stresses in an Abdominal Aortic Aneurysm using Viscoelastic Model

Author: Ningxin Qiao

Supervisor: Prof. Rosaire Mongrain

Prof. Evgeny Timofeev

Department of Mechanical Engineering

McGill University

Montreal, Canada

December 7th, 2020

A thesis submitted to McGill University in partial fulfilment of the requirements of the

Undergraduate Honours Program

Abstract

An attempt was made to evaluate the wall stresses in an abdominal aortic aneurysm using viscoelastic model. In this research, a 3D aneurysm model was reconstructed from the CT scan slices and then imported to Ansys Mechanical (ANSYS Inc. Canonsburg, PA, USA) for finite element analysis. The geometry stored in a STL file was first parametrized using the reverse engineering tools in SpaceClaim, and the viscoelastic properties of the material was defined using the Prony series to fit the experimental data. The aorta surface was discretized with quadrilaterals because of its complex shape, and the mesh was refined using the convergence tool. One heart cycle was simulated under two different scenarios: at rest and during exercise. It was observed from the proposed mathematical modelling that the peak stress occurred at the end of systole at both necks of the aneurysm. The peak stress during the exercise was much higher than the one at rest; and compared to the linear elastic model, the wall experienced a larger strain under the same pressure load and a lower stress for a given strain with the viscoelastic model. In a nutshell, the use of viscoelastic properties gave a better estimation of arterial wall stress in aneurysm.

Abrégé

Une tentative a été faite pour évaluer les contraintes de paroi dans un anévrisme de l'aorte abdominale en utilisant un modèle viscoélastique. Dans cette recherche, un modèle d'anévrisme 3D a été reconstruit à partir des tranches de tomodensitométrie puis importé vers Ansys Mechanical (ANSYS Inc. Canonsburg, PA, USA) pour effectuer la méthode des éléments finis. La géométrie stockée dans un fichier STL a été d'abord paramétrée à l'aide des outils d'ingénierie inverse de SpaceClaim, et les propriétés viscoélastiques du matériau ont été définies à l'aide de la série Prony ajustant les données expérimentales. La surface de l'aorte a été discrétisée avec des quadrilatères en raison de sa forme complexe, et le maillage a été affiné à l'aide de l'outil de convergence. Un cycle cardiaque a été simulé sous deux scénarios différents: au repos et pendant l'exercice. Nous avons observé à partir de la modélisation mathématique proposée que le pic de contrainte s'est produit à la fin de la systole aux deux cols de l'anévrisme. La contrainte maximale pendant l'exercice était beaucoup plus élevé que celle au repos; et par rapport au modèle élastique linéaire, la paroi a subi une déformation plus importante sous la même charge de pression et une contrainte plus faible pour une même déformation avec le modèle viscoélastique. En bref, l'utilisation de propriétés viscoélastiques a pu donner une meilleure estimation de la contrainte de la paroi artérielle dans l'anévrisme.

Acknowledgements

I would first like to thank my thesis supervisor Prof. Rosaire Mongrain for giving this great opportunity to work on this research project, as well as his continuous encouragement and support. The door to Prof. Mongrain office was always open whenever I ran into a trouble spot or had a question about my research. He consistently allowed this paper to be my own work, but steered me in the right the direction whenever he thought I needed it.

I would also like to acknowledge Prof. Evgeny Timofeev as the second reader of this thesis, and I am gratefully indebted to his validation of this research project, as well as his very valuable comments on this thesis.

I would also like to thank the PhD candidate Mr. Stewart McLennan for giving me all the necessary materials to start this project, as well as his guidance and feedback. Mr. McLennan's knowledge was key to allow me having a better understanding of the materials at my hand, and this thesis has also benefited from his comments and suggestions.

Finally, I must express my very profound gratitude to my parents and friends for providing me with unfailing support and continuous encouragement throughout my years of study and the process of research and writing this thesis. This accomplishment would not have been possible without them. Thank you.

Ningxin Qiao

Table of Contents

List of Figures

List of Tables

1 Introduction

1.1 Background

According to the World Health Organization, cardiovascular diseases are the number 1 cause of death globally, taking an estimated 17.9 million lives each year. Among them, there is aortic aneurysm. An aortic aneurysm is an enlargement dilatation of the aorta to greater than 1.5 times normal size. They usually cause no symptoms except when ruptured. A sudden rupture can cause life-threatening internal bleeding. In general, a surgery is needed when the risk of rupture is too high. However, the surgery may include heart-related problems, swelling or infections at the site, or respiratory infections, with a mortality of 5% [1]. Therefore, an appropriate assessment of the state of aortic is essential to avoid rupture and non-necessary surgery.

It is widely believed that larger diameter of aorta leads to a stiffening of the wall stress, and thus a sudden rupture. For this reason, currently surgical decision making is widely based on maximal aneurysm diameter. However, clinical experiments showed that aneurysms smaller than the current guidelines are also known to rupture on an unpredictable basis, and no direct relationship between the diameter of the aorta and its wall stress has been discovered yet [2]. Therefore, a better understanding of mechanical properties of the aorta is essential for a better prediction.

To achieve this, some research has already been directed into numerical modelling and analysis. The 3D aorta model is in general reconstructed from the CT scan slices, and the mechanical properties of the aorta tissues are assessed using *in vitro* mechanical tests, uniaxial or biaxial.

1.2 Viscoelasticity of Aortic Wall

Each cardiac cycle can be divided into two parts: systole and diastole. During systole, the heart pumps oxygenated blood from the left ventricle through the aortic valve and aorta to all body systems. During diastole, the heart stops contracting, and the aortic valve is closed and prevents backflow. If the aortic wall was rigid, the blood would stop flowing. However, since the aorta has compliance, it would dilate during systole due to the blood pressure leading to the elastic stretching of the walls. The potential energy is then stored in the deformed wall. During diastole, the aortic wall collapses back in, releasing the potential energy and pushing the blood to continue to flow. This is known as Windkessel effect modelled by a two-element circuit, where P represents the heart pump, C and R represent the compliance and the resistance of the aortic wall respectively [3].

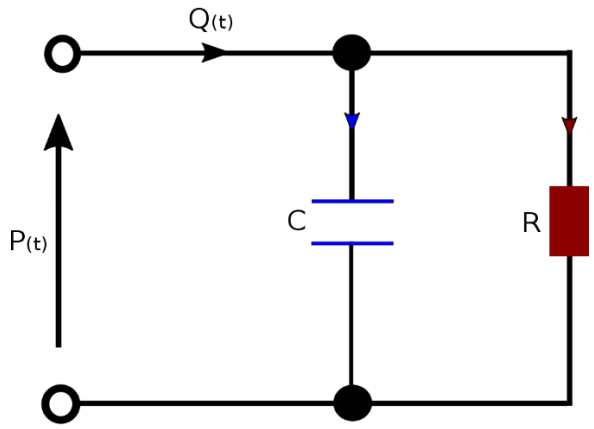

Figure 1 Two-element Windkessel circuit analogy illustrated

The aortic wall dissipates some energy into itself during each cardiac cycle, and not all the energy received from the pumping heart is restored back to the blood flow. Consequently, the blood pressure is lower, and the aorta cannot stretch back to its original shape. This is known as energy loss, which is related to the viscosity of the material [4]. Hysteresis (Area A in Figure 2) is observed in the stress–strain curve, with the area of the loop being equal to the energy lost

during the loading cycle.

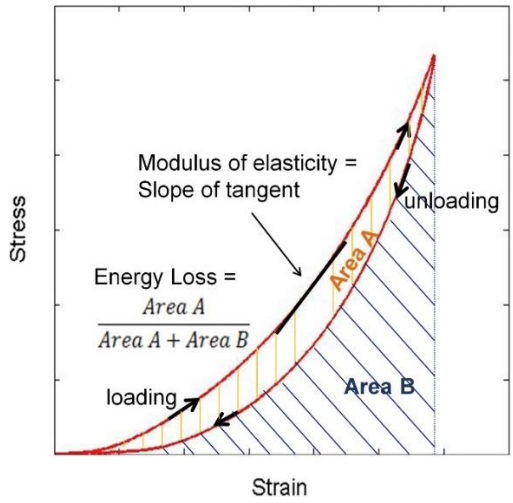

Figure 2 True stress-strain relationship of an arterial cell

The aorta wall is generally known as a viscoelastic material because it exhibits both viscous and elastic characteristics when undergoing deformation. Evaluating the material properties correctly is key for a good estimation of the aortic wall peak stress.

1.3 Elastic Properties

The concept of a longitudinal elastic modulus, commonly referred to as Young's modulus, was introduced during the first decade of the 19th century to describe the aggregate elastic characteristics of arterial wall constituents and structure [5]. A method to obtain its value consists of using noninvasive ultrasonic pulse-echo tools to determine with high precision the variables that define Young's modulus. The relationship between Young's modulus and the parameters are defined as:

$$E = \frac{D}{2w}\frac{P}{t} \tag{1}$$

where E is Young's modulus, D the arterial diameter, w the wall thickness, P the pulse pressure, and t the fractional increase in arterial diameter during the cardiac cycle.

The Young's modulus, as well as the wall thickness of 3321 human arteries were determined [6]. The values of both parameters were patient specific, and it was found that an aortic aneurysm with larger diameter would result in a larger value of Young's modulus. In the present study, the mean Young's modulus and the wall thickness of aorta were assumed to be 840 kPa and 2 mm respectively.

Another important parameter of an elastic material is the Poisson's ratio, which is a measure that describes the expansion or contraction of a material in directions perpendicular to the direction of loading. To evaluate its value, rectangular sections comprised of the intimal and medial layers were excised from the descending aorta, loaded in displacement control uniaxial tension up to 40% elongation [7], and both the axial strain ϵ_{axial} and the transverse strain ϵ_{trans} were measured. The Poisson's ratio ν was approximated by:

$$\nu = -\frac{\epsilon_{trans}}{\epsilon_{axial}} \tag{2}$$

An average value of 0.45 was found, which confirmed the quasi-incompressible property of the aortic wall due to its high water content.

1.4 Viscous Properties

To measure viscoelasticity, the time-dependent mechanical behaviour of a material must be measured. It can be quantified with stress relaxation experiments that are conducted by applying a constant strain and measuring the decrease in stress as a function of time [4]. Typically, a preconditioning is performed before data collection, and the goal is to induce a pseudoelastic state in which the tissue structure no longer changes with cyclic loading, resulting in a consistent mechanical response to a load or deformation.

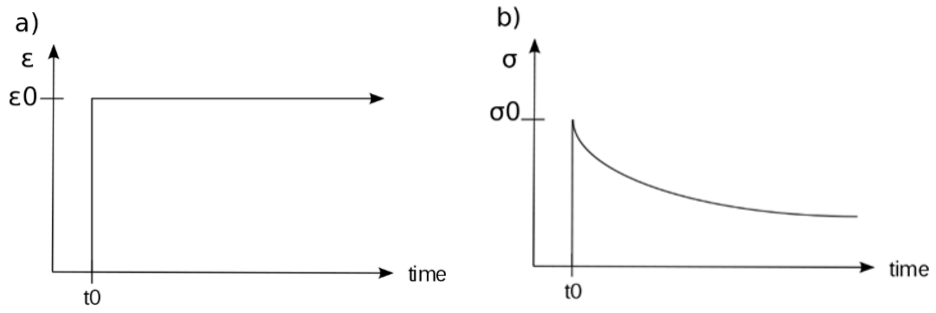

Figure 3 a) Applied strain and b) Induced stress as functions of time for a viscoelastic material.

In general, human aortic tissues are required for the experiments. However, the use of human tissues is only allowed in special occasions and it must be approved by the research ethics committee. Under this context, a biocompatible hydrogel called "polyvinyl alcohol (PVA)" is widely used in many biomedical applications. PVA is a hydrophilic polymer that was shown to display non-linear isotropic mechanical properties as well as viscoelastic behaviour, matching the mechanical response of selective cardiovascular tissues [8].

To evaluate the viscous properties of an aortic tissue, a biaxial tensile test on a $10 \times 10 \times 3.75\ mm^3$ 10% PVA (10% PVA and 90% water) patch was used to perform the stress relaxation test, with 10 cycles of preconditioning and 5 of stress-relaxation. The test was performed by a group of researchers at McGill University. A 60% strain was applied to each cycle of stress-relaxation for 2000 s. The load needed to hold the patch was recorded as a function of time. Due to its isotropic properties, only the data along one direction was plotted and used for analysis in this research.

1.5 Thesis Objective and Outline

Various attempts were made to evaluate the effects of aortic wall stress using Finite Element Analysis (FEA). Until the present day, purely elastic material properties were assumed in most FEA analyses. While they greatly accounted for the stress variations of the aortic wall

due to the change of geometry, one must bear in mind that viscoelasticity of the aorta tissues affects temporal variables and is associated with irreversible energy loss. Therefore, it passively controls the synchronization of events (Windkessel effect) and affects the wall stress.

With the scholarly sources of the existing research presented in the previous sections of this chapter, it was possible to construct a viscoelastic material model. In this research, both purely isotropic and viscoelastic models were used under two different scenarios: at rest, and during exercises. The aortic wall stresses were evaluated in the above cases for comparison.

The rest of the paper contains three chapters. In Chapter 2, the setup of FEA model will be presented, including the geometry preparation, material definition, mesh analysis and FEA setup. The results of the two scenarios using both models will then be presented and discussed in Chapter 3. Finally, the paper will be summarized and the future work will be suggested in Chapter 4.

2 Method

2.1 Geometry

2.1.1 Geometry Acquisition

In this research, we needed a 3D AAA model that had to be anatomically correct with a root aneurysm, ranging from the renal artery to the common iliac arteries. After defining the region of the study, the adequate medical imaging process was used by a radiologist to obtain the imaging data for an appropriate representation. A multitude of CT scan slices with 1 mm spacing were taken and stacked into successive layers [9], and the missing volume was filled using linear extrapolation. Each CT scan slice was analyzed individually, and data points were created along the perimeter to define the boundary. The point clouds were then connected to create the surface of the object.

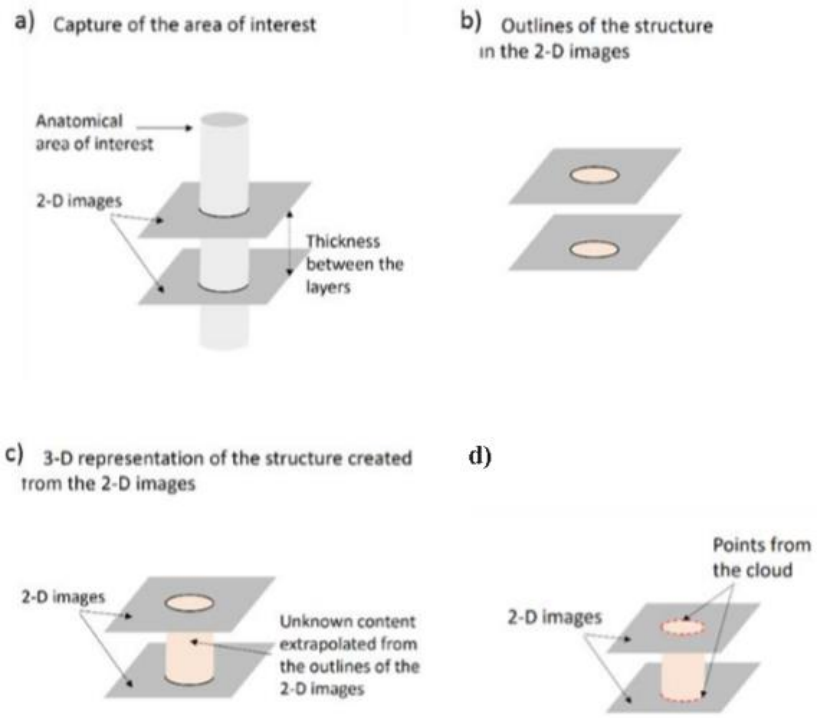

Figure 4 Procedures of geometry acquisition [10]

The interconnected elements of the model presented surface irregularities or sharp edges

that needed to be removed. Most irregularities were fixed by smoothing the surfaces with algorithms. In general, too little smoothing generally increases the number of elements required to define the object, increasing the file size [10]. The file size was controlled to be 6,500 KB during the smoothing to avoid long processing time and unnecessary details. Finally, repair algorithms highlighted and corrected all potential errors in the meshes before exporting the model as an STL file for further processing.

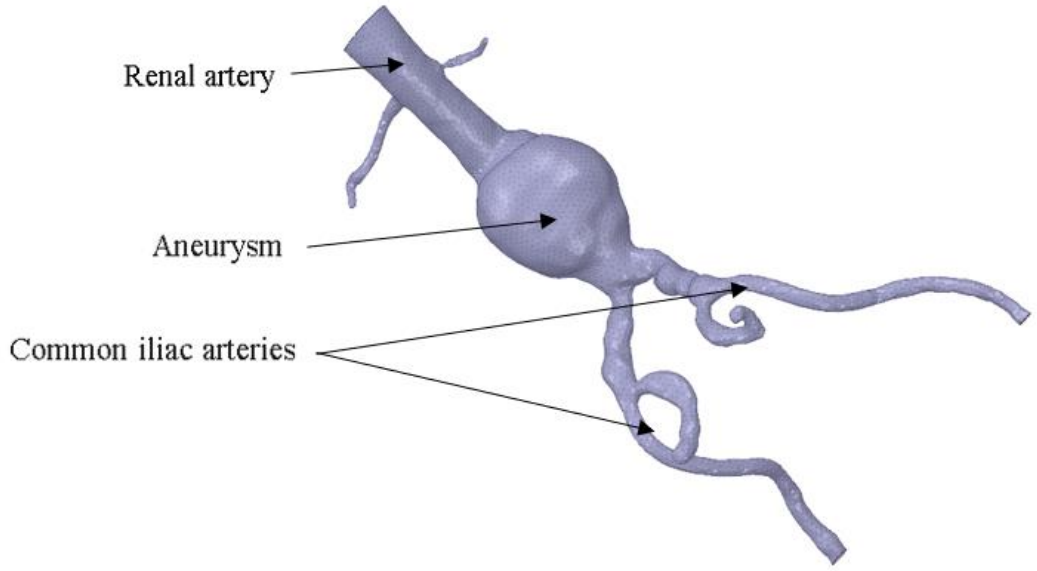

Figure 5 Aorta model in STL format

2.1.2 Geometry Parametrization

An STL file uses a series of linked triangles to recreate or reproduce surface geometry of the 3D model. Consequently, it is not able to capture geometry appropriately and the use of it will result in meshing error in FEA. This encouraged us to convert it into a computer aided design (CAD) model which uses mathematical expressions to define curves that control the object's surfaces. As they are easy to manipulate, they can then be used in simulations.

A groundbreaking tool in SpaceClaim (ANSYS Inc. Canonsburg, PA, USA) called "Skin Surface" was used in this research for the geometry parametrization of the aorta model. It is a

powerful method for autosurfacing to surface or solid geometry from prismatic shapes. It uses multiple control points to define non-uniform rational basis splines (NURBS), a mathematical model with great flexibility and precision for generating and representing curves and surfaces. All the NURBS delimited by the boundaries define the shape of a surface that approximates the original model. Since the triangles in the stereolithography (STL) file form a rough surface, the approximate method is used in most cases for smoothing purposes.

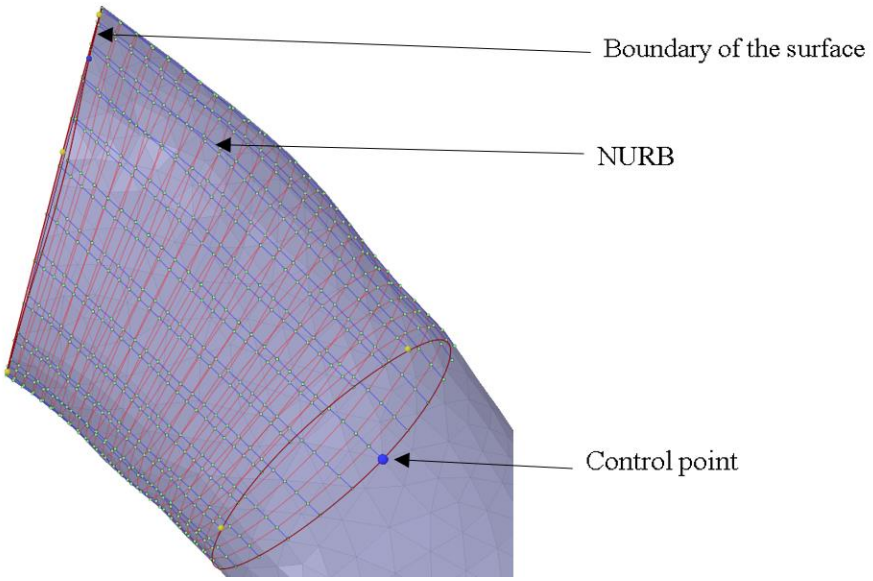

Figure 6 Example of surface parametrization

Our entire aorta model was divided into multiple faces connected at the boundaries. Since the model had a shape of a pipe, the best way to divide it was to use circular boundaries as shown in Figure 6. The distance between both boundaries of a surface could be as long as possible provided that the control points were close to the surface of the original model. If the control points deviated from the model, one would have to consider using more surfaces with closer boundaries to avoid an altered geometry. This usually occurs when the geometry of the aortic vessel changes significantly, for example at junctions or elbows.

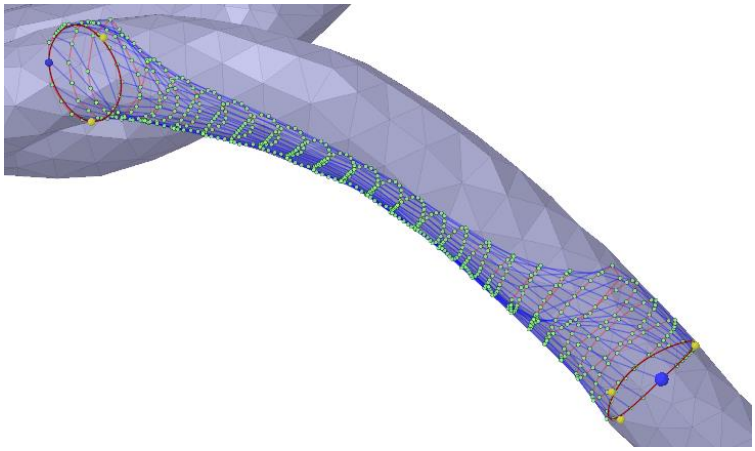

Figure 7 Example of poorly defined surface boundaries

Despite the previous smoothing process presented in 2.1.1, irregularities may still be present and they can be a source of an unnecessary mesh concentration. Therefore, it is advisable to manually smoothen the area. One common way to achieve this is by deleting the existent irregular surfaces and then filling the missing surface with a simplified geometry.

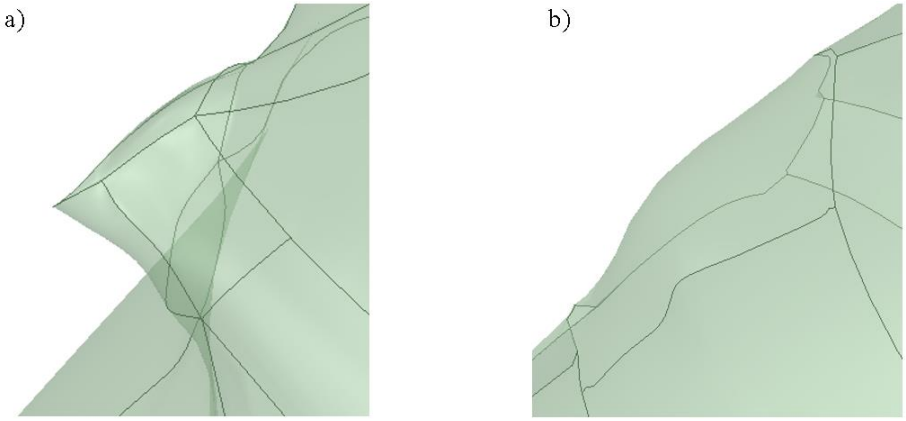

Figure 8 a) Before surface smoothing b) After surface smoothing

Regardless of sharp corner and edges, the CAD model must correctly represent the original model, especially in the aneurysm part. The deviation tool was used this analysis to see how close the geometry of the STL model and the CAD model matched up. The deviation was set to be 0.01 mm, and despite large deviations in smoothened areas, the whole STL model was correctly parametrized and the aneurysm part was within the tolerance. The CAD model was valid and ready for use.

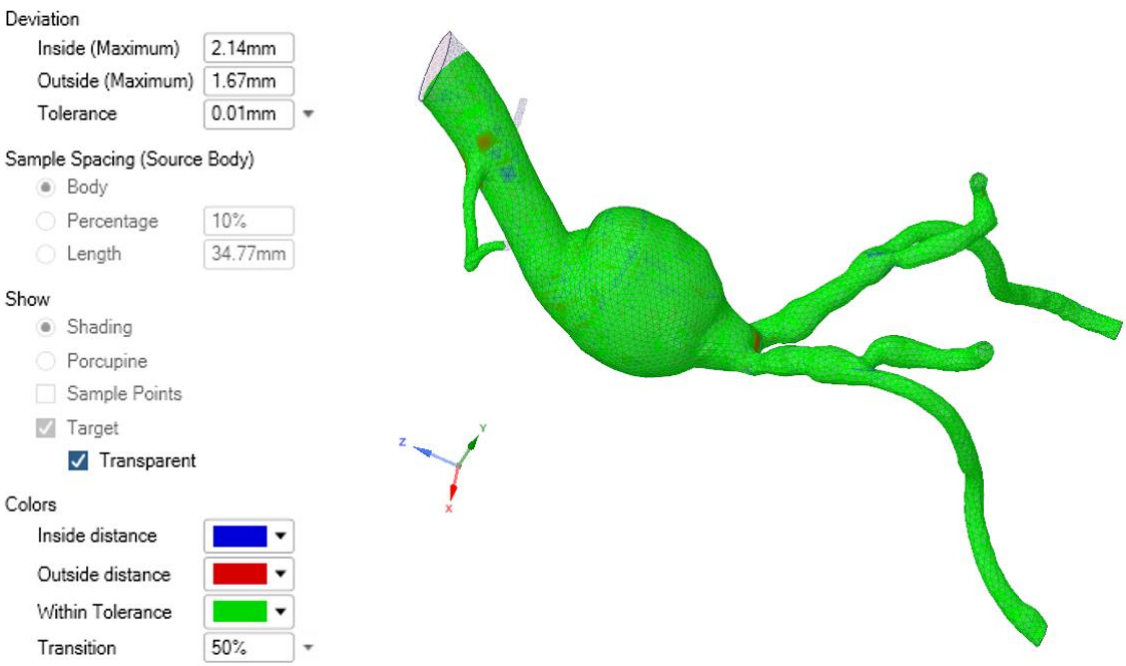

Figure 9 Deviation check of the CAD model

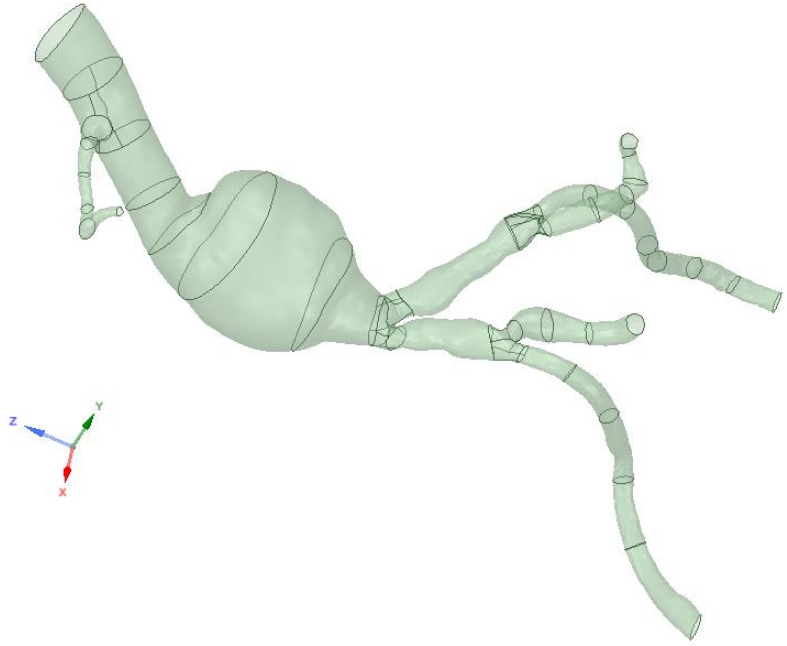

Figure 10 CAD model of AAA

2.2 Material Definition

2.2.1 Derivation of Prony Shear Series

The viscoelastic properties of a AAA wall can be modelled by n pairs of spring-dashpot in parallel known as Maxwell–Wiechert model. A representation of this model is shown as below where E is the elastic modulus of the spring and η the viscosity of the dashpot.

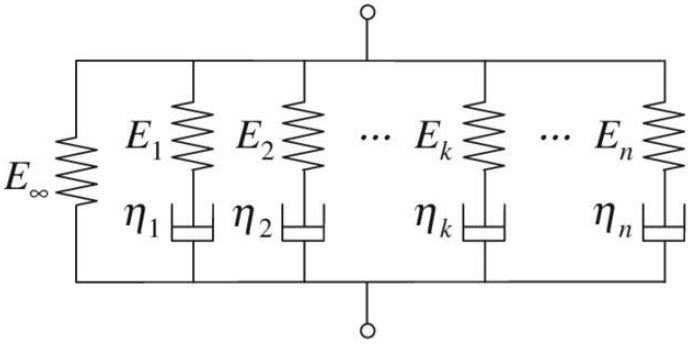

Figure 11 Schematic of generalized Maxwell–Wiechert model

The mathematical expression of this model is needed for FEA. First, derive the expression for one single spring-dashpot pair using E_1 and η_1.

The stress due to the spring is

$$\sigma_1(t) = E_1 \epsilon_s(t) \tag{3}$$

The stress due to the dashpot is

$$\sigma_1(t) = \eta_1 \frac{d\epsilon_D(t)}{dt} \tag{4}$$

where σ_1 is the stress applied to the first spring-dashpot pair, ϵ_s the strain due to the spring, and ϵ_D the strain due to the dashpot. Using Laplace transform, the equation (3) remains the same and the equation (4) becomes

$$\sigma_1(s) = s\eta_1 \epsilon_D(s) \tag{5}$$

The total resultant strain ϵ is the sum of both strains, and using equations (3) and (5)

$$\epsilon(s) = \epsilon_s(s) + \epsilon_D(s) = \frac{\sigma_1(s)}{E_1} + \frac{\sigma_1(s)}{s\eta_1} \tag{6}$$

During the stress-relaxation test, the strain is held constant overtime for all $t \geq 0$, and stress free otherwise. Neglecting the time required to step up the strain from 0 to ϵ_0 at $t = 0$, the expression of the strain in time domain is

$$\epsilon(t) = \epsilon_0 H(t) \tag{7}$$

where H is the Heaviside step function. The Laplace transform of equation (7) is

$$\epsilon(s) = \frac{\epsilon_0}{s} \tag{8}$$

Combining and arranging equations (6) and (8), one obtain

$$\epsilon_0 = \frac{s\sigma_1(s)}{E_1} + \frac{\sigma_1(s)}{\eta_1} = \frac{\eta_1 s + E_1}{E_1\eta_1}\sigma_1(s) \tag{9}$$

Therefore,

$$\sigma_1(s) = \epsilon_0 \frac{E_1\eta_1}{\eta_1 s + E_1} = \epsilon_0 E_1 \frac{1}{s + \frac{E_1}{\eta_1}} \tag{10}$$

Let $\tau_1 = \eta_1/E_1$ be the time constant, and apply the inverse of Laplace transform,

$$\sigma_1(t) = \epsilon_0 E_1 e^{-\frac{t}{\tau_1}} \tag{11}$$

Since all the pairs of spring-dashpot are in parallel, the total stress σ is the sum of the stresses applied at each pair:

$$\sigma(t) = E_\infty \epsilon_0 + \sum_{k=1}^{n} \epsilon_0 E_k e^{-\frac{t}{\tau_k}} \tag{12}$$

For a homogeneous isotropic material as PVA, we apply the equation

$$G = \frac{E}{2(1+\nu)} \tag{13}$$

where ν is the Poisson's ratio of the material. Therefore, dividing the equation (12) by $2(1+$

$\nu)\epsilon_0$ and factor the equation by G_0, one can obtain

$$G(t) = G_0(\alpha_\infty + \sum_{k=1}^{n} \alpha_k e^{-\frac{t}{\tau_k}}) \tag{14}$$

where $\alpha_k = G_k/G_0$ and $\alpha_\infty = G_\infty/G_0$ are the relative moduli. The equation (14) called "Prony shear series" was used in this research to fit the experimental data of the stress-relaxation test of 10% PVA in order to model the viscoelastic properties of aortic tissues. With G_0 and G_∞ known, we had to determine the values of Prony pairs α_k and τ_k.

2.2.2 Determination of the Coefficients of Prony Shear Series

To apply the fit using equation (14), we must obtain the data set of the instantaneous shear moduli from the force data. First, the instantaneous Young's modulus E is defined as

$$E(t) = \frac{\sigma(t)}{\epsilon_0} = \frac{L}{A\delta_0} F(t) \tag{15}$$

where F is the load, L the original length, A the cross-section area and δ_0 the displacement. The shear moduli can be then obtained using equation (13).

To find the optimal values of the Prony pairs, the error function of the Prony shear series was used to evaluate the quality of the curve fit. Starting with one-term Prony shear series, the error function χ_1^2 is defined as

$$\chi_1^2(\alpha_1, \tau_1) = \sum_{i=1}^{N} [G_i - G(t_i, \alpha_1, \tau_1)]^2 \tag{16}$$

where N is the number of the experimental points, G_i and t_i the experimental data, and G_1 and τ_1 the unknown constants. Using the solver tool in Microsoft Excel (Redmond, WA, USA), we were able to find the optimal Prony pair when the error function was minimized.

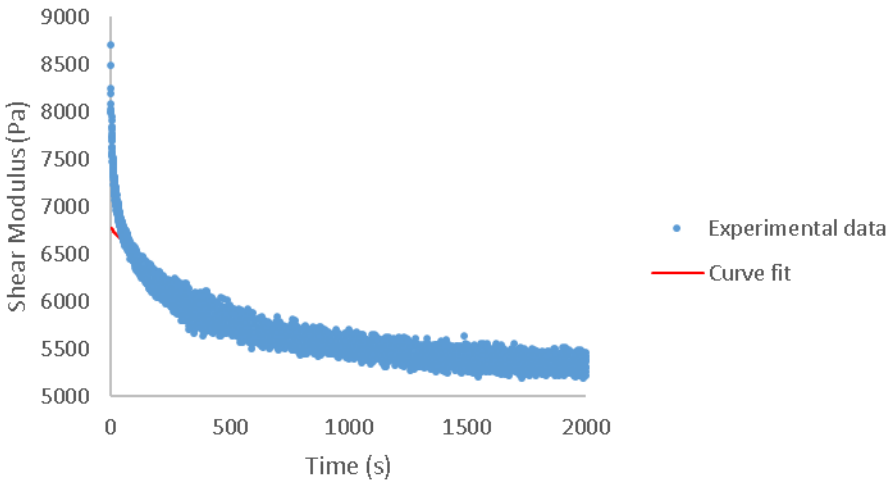

Figure 12 Curve fitting with one Prony pair

With $G_0 = 8720$ kPa and $G_\infty = 5230$ kPa, the one-term Prony series approximation was found with $\alpha_1 = 0.1766$ and $\tau_1 = 545.65\,\mathrm{s}$. Unfortunately, the curve fit was not accurate enough at the start of the stress-relaxation test. In fact, at $t = 0$, the equation (14) becomes

$$G(0) = G_0(\alpha_\infty + \sum_{k=1}^{n} \alpha_k) \tag{16}$$

In other words, the sum of the relative moduli α_k must be equal to 1 to represent the full stiffness. However, the one term approximation only gave a total stiffness of

$$\alpha = \alpha_\infty + \alpha_1 = \frac{G_0}{G_\infty} + \alpha_1 = 0.7766 \tag{17}$$

Therefore, more terms had to be used to give a better approximation.

With 6-term approximation, we obtained a total stiffness of $\alpha = 0.9991$ which was accurate enough. A residual plot was also used to assess the quality of the curve fit. It is a graph that shows the error of the fit on the vertical axis and the independent variable on the horizontal axis. The points in the residual plot were randomly dispersed around the horizontal axis, indicating a good fit.

α	τ (s)
0.096637	951.4216
0.094727	174.2911
0.065377	0.527335
0.037223	25.43139
0.037223	25.43151
0.067948	5.337961

Table 1 Prony pairs

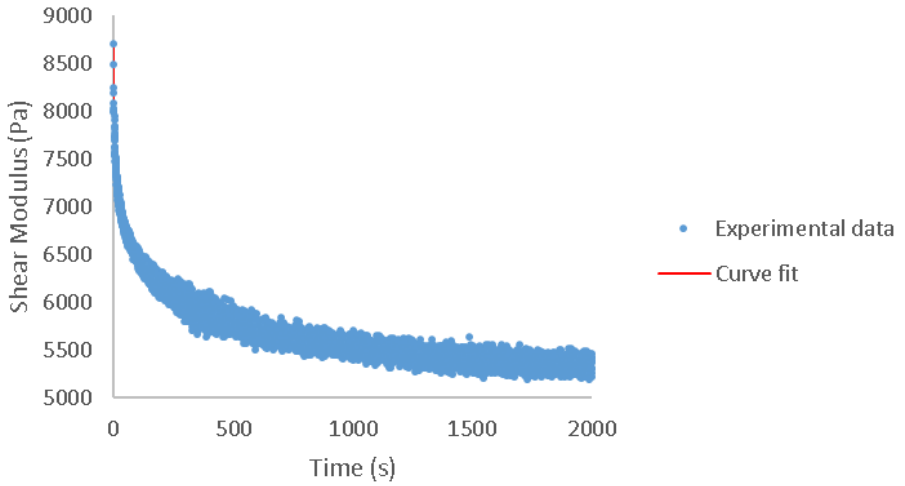

Figure 13 Curve fitting with 6 Prony pairs

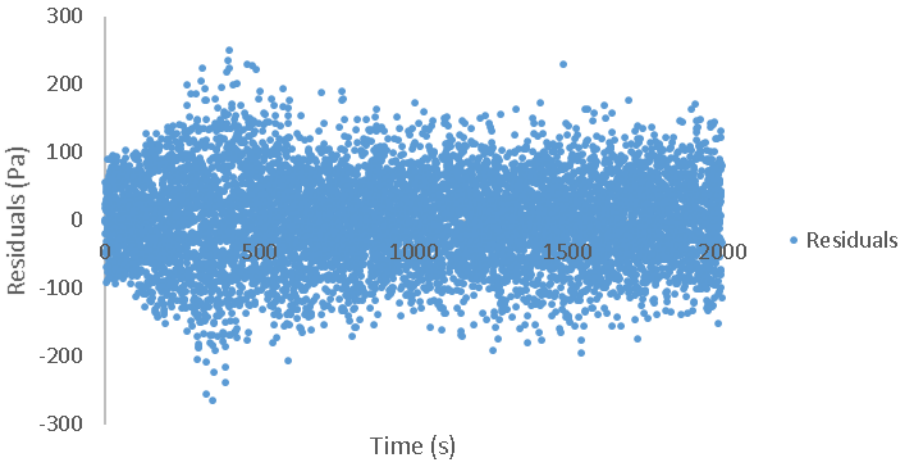

Figure 14 Residuals of the curve fitting with 6 Prony pairs

2.3 Mesh

The entire model was meshed with quadrilaterals (quads). Quad mesh is very useful for fitting NURBS: one spline patch is defined for each regular patch of the mesh, and different patches are glued together at common boundaries. It can act as control meshes for subdivision surfaces that provide base shapes for arbitrarily complex objects and characters [11]. In addition, it is also preferred within highly elastic and plastic domains, for which they reduce both the approximation error and the number of elements as compared to triangles [12].

The default defeaturing and curvature capture sizes were set to be at the order of 10^{-5} m in Ansys Mechanical. In other words, a geometry change or curvature variation larger than this value needed to be counted in meshing. This tolerance was too tight, because the meshing time was excessively long and the mesh element number excessively high. To optimize the meshing process, both parameters were set to be 0.002 m and the element size was 0.003 m.

Element size	0.003 m
Growth rate	1.2
Mesh defeaturing size	0.002 m
Curvature minimum size	0.002 m
Curvature normal angle	30°
Bounding box diagonal	0.34508 m
Average surface area	0.00057606 m
Minimum edge length	0.000035531 m
Target quality	0.5
Smoothing	Medium
Transition ratio	1.2
Maximum layers	2

Table 2 Mesh setup

Before jumping into the next step, it was important to check the mesh quality especially as the mesh was relatively coarse. Two main criteria were used in the simulations: skewness and aspect ratio.

Skewness is defined as the difference between the shape of the cell and the shape of an

equilateral cell of equivalent surface. Highly skewed cells can decrease accuracy and destabilize the solution [13]. A maximum value above 0.95 may lead to convergence difficulties and may require changing the solver controls. Generally, the average value should be less than 0.33. In the meshing of the AAA model, the average skewness was 0.12 with most elements having a skewness less than 0.05.

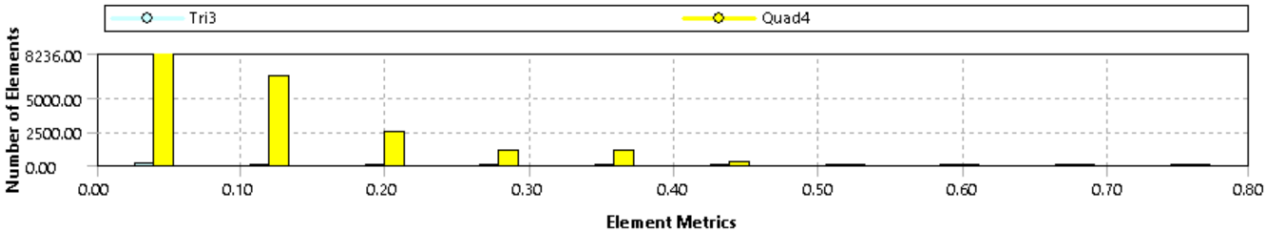

Figure 15 Skewness distribution of mesh elements

Aspect ratio is a measure of the stretching of the cell, defined as length to height ratio for a surface element. FEA theories state that local variation in cell sizes should be minimal citing that large aspect ratios can result in interpolation errors of unacceptable magnitudes and loss of computational accuracy. Therefore, the best possible value of the aspect ratio for an element is 1. A rough guideline suggests that elements with aspect ratios exceeding 3 should be viewed with caution. In our model, the ratio of most of the elements was very close to 1.

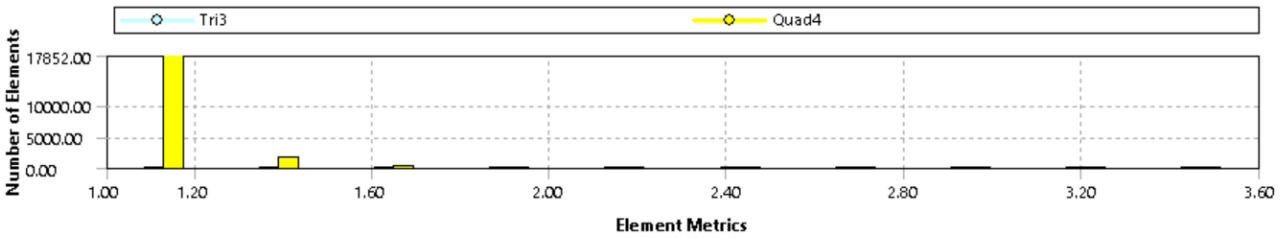

Figure 16 Aspect ratio distribution of mesh elements

	Skewness	Aspect ratio
Min	0.00091577	1
Max	0.79738	3.6024
Average	0.12231	1.1166
Standard deviation	0.095802	0.11493

Table 3 Summary of mesh quality

As the mesh elements are made smaller and smaller, the mesh is refined and the

computed solution will approach the true solution. However, this process also makes the model more complex and requires more time and memory for the FEA. Therefore, a good mesh refinement at the key areas is essential to find the balance between the solution accuracy and the computational cost. In general, the element concentration is higher in areas where large deformations were found to occur [14]. A convergence monitor permits an automatic mesh refinement at the critical areas, and the mesh is considered to be sufficiently refined if the change in maximum displacement is within 5% before and after the refinement. For a better accuracy, a threshold of 3% was imposed in this research, and two iterations were enough to reach the convergence. A slight increase of displacement was observed after the refinement, indicating a better accuracy of the solution.

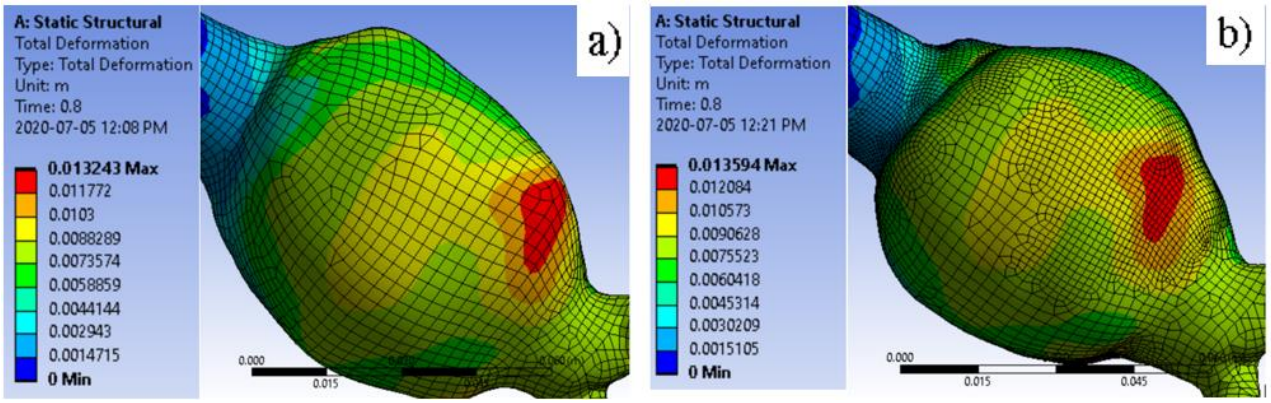

Figure 17 a) Before mesh refinement b) After mesh refinement

	Total Deformation (m)	Change (%)	Nodes	Elements
1	1.3243e-002		6999	7022
2	1.3594e-002	2.6145	10852	10886

Table 4 Summary of mesh refinement

2.4 FEA Setup

Two constraints were defined in this setup: fixed support and pressure. The fixed supports were applied to the edges on the boundaries of the model to provide stability; and the pressure was applied to all the surfaces. Since it was a surface model, there was no distinction between applying the pressure load from inside or outside the surface.

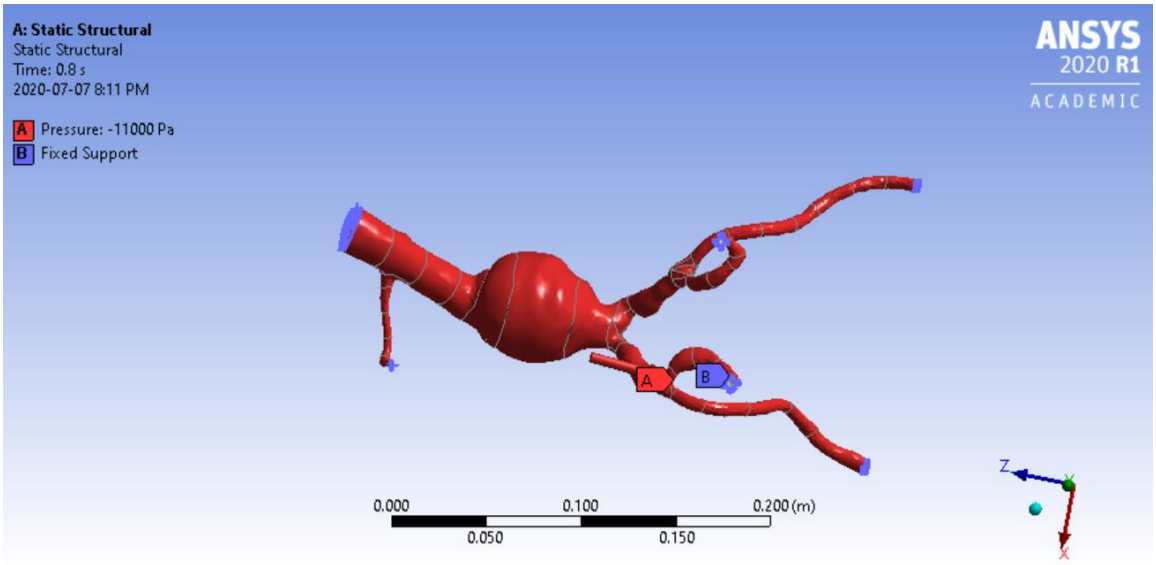

Figure 18 Boundary conditions of the AAA model

Two scenarios were considered in this research, at rest and during exercise. A person's blood pressure is between 80 mmHg and 120 mmHg at rest, and between 84 mmHg and 155 mmHg during exercise [15]. It was assumed a normal heart rate of 75 beats per minute at rest, and 150 beats per minute during exercise. The systole region was assumed to represent the first ¼ of a heart cycle, and the diastole the remaining ¾ of the cycle.

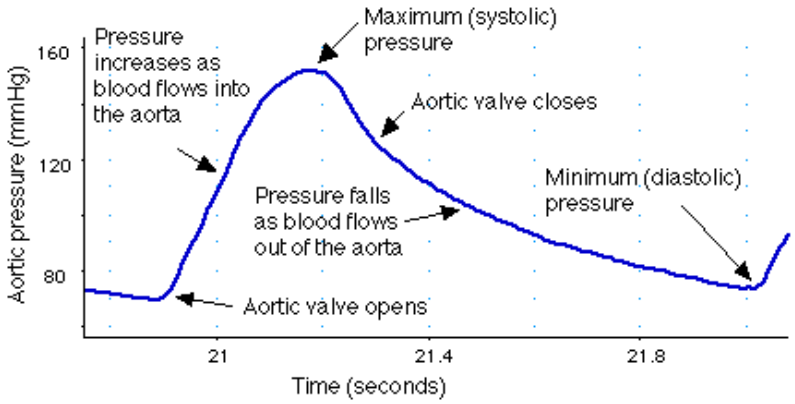

Figure 19 Arterial pressure waveform

The pressure variation during systole and diastole was modelled with two different sinusoidal waves joined at the peak pressure. The amplitude was defined by the difference between the highest and lowest pressures. The sine wave during either systole or diastole represented ¼ of a period of the curve. The sine waves were of the form

$$P = Asin\left(\frac{2\pi t}{T} + \alpha\right) + B \tag{18}$$

where P is the pressure, t the time, A the amplitude, ω the angular frequency, α the phase shift and B the offset. Notice that P is the dependent variable, t the independent variable, and A, T, α, B a set of parameters tabulated as below. The parameter α ensures the continuity of the curve at the peak pressure, and the parameter B ensures the correct pressure range.

	A (kPa)	T (s)	α (°)	B (kPa)
Systole – at rest	5.4	0.8	0	10.6
Diastole – at rest	5.4	2.4	60	10.6
Systole – during exercise	9.6	0.4	0	11.0
Diastole – during exercise	9.6	1.2	60	11.0

Table 5 Parameters that define various pressure profiles

One cardiac cycle was modelled for both scenarios. For discretization, a 0.01 s time interval was used for a heartbeat at rest and 0.005 s time interval was used for a heartbeat during exercise.

3. Result and Discussion

3.1 Overall Behaviour

The deformation was recorded for mesh refinement presented in section 2.3. Von Mises criterion was used because the aortic wall was assumed to be isotropic and subjected to a complex loading condition.

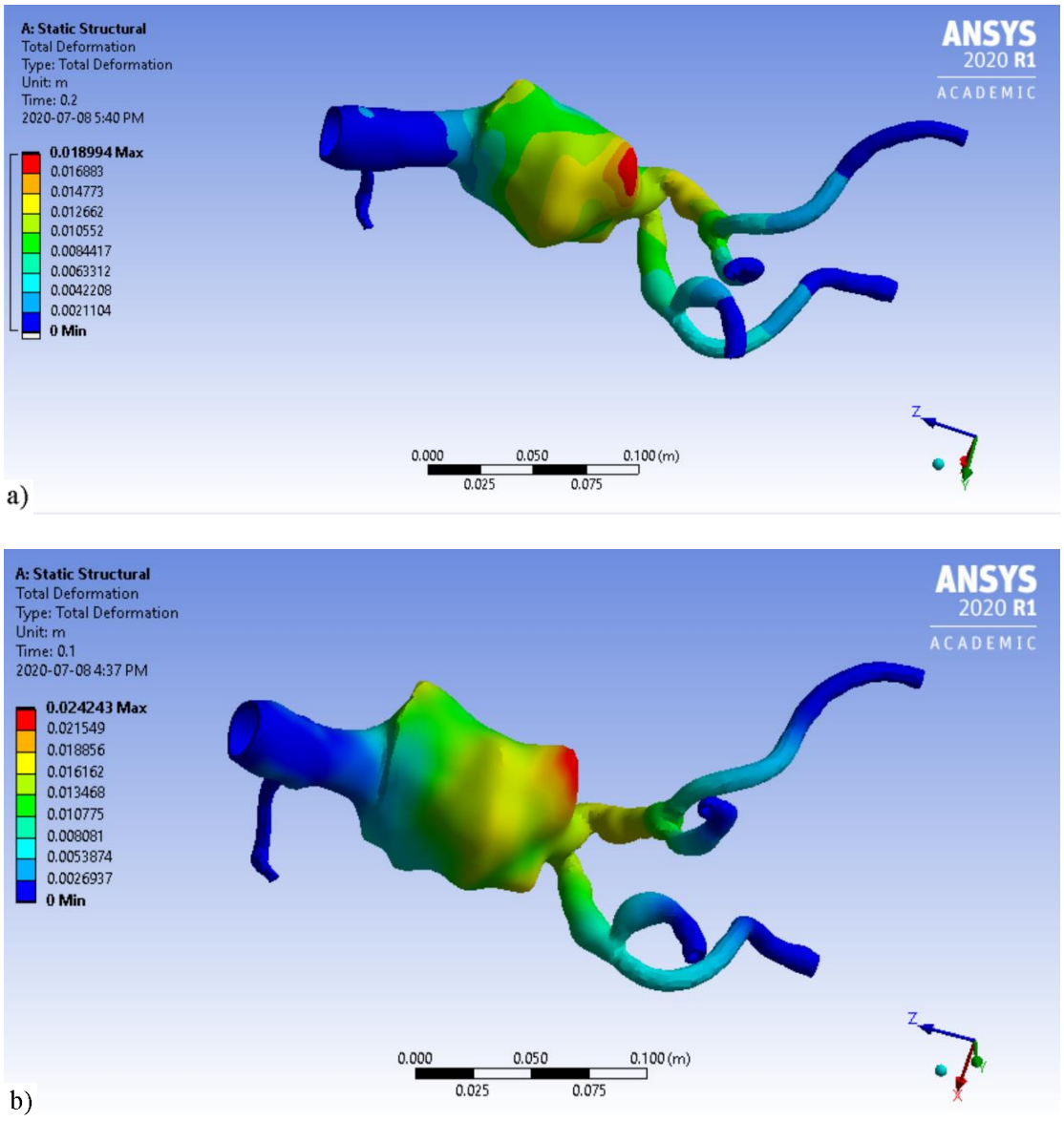

Figure 20 Displacement at peak pressure load a) at rest b) during exercise

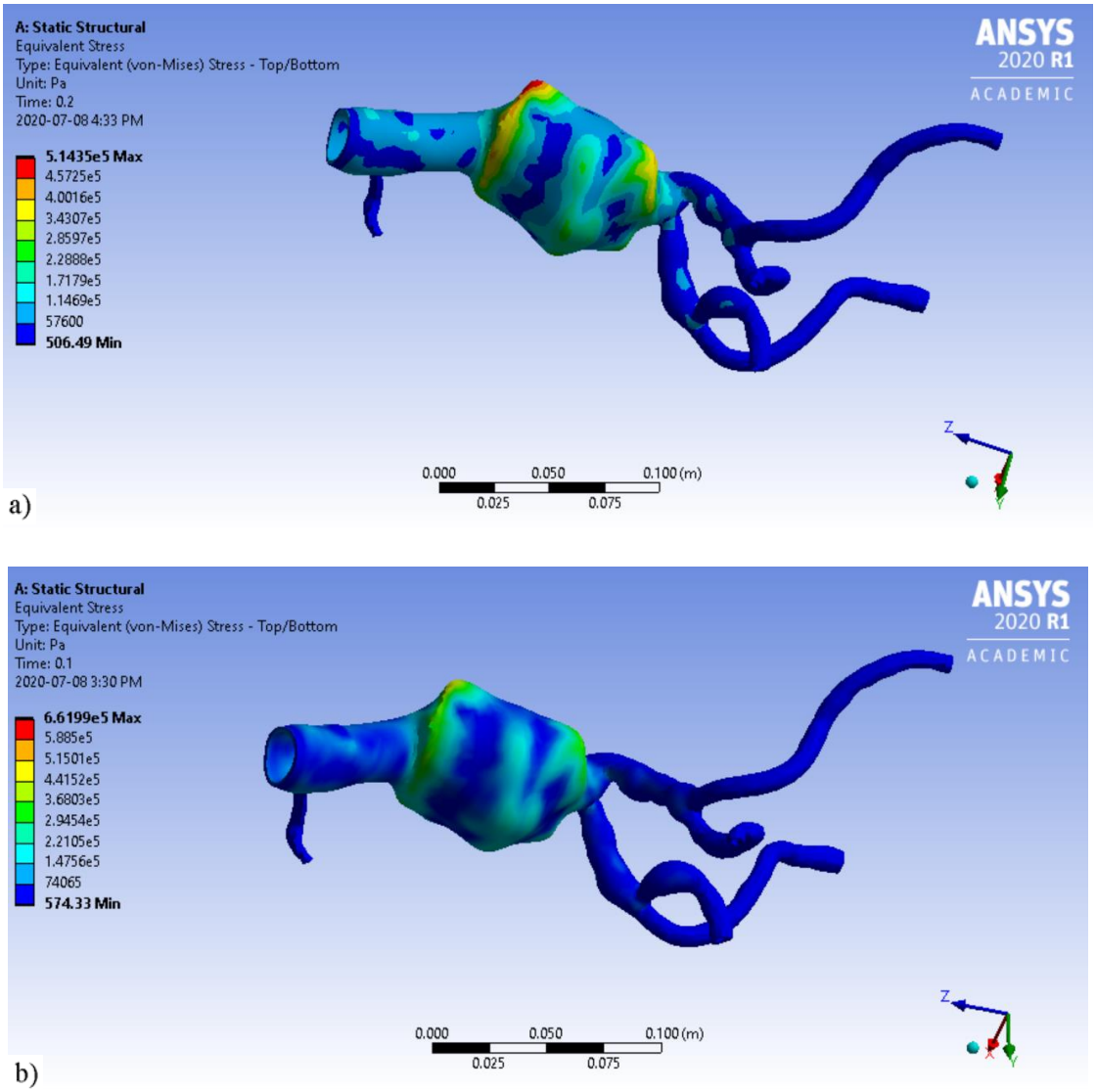

Figure 21 Equivalent stress at peak pressure load a) at rest b) during exercise

In both cases, the peak wall stress found on the surface of the AAA model occurred at the end of systole, at both necks of the aneurysm, with a value of the order of 10^5 Pa. The similar result was also found previously using hyperelastic model, confirming the validity of the current model [16]. Notice that the deformations were not circular, and the largest displacement and the highest wall stress did not occur at the same position. This showed that the current clinical practice using the maximum diameter of the aneurysm as a predictor for AAA rupture was not accurate, and the FEA could give a better estimation of the stress state.

3.2 Stress Distribution

To study the distribution of stress on the wall at the critical regions, we plotted the Von Mises stress along three paths on the AAA surface at the end of a heart cycle: a longitudinal path (green curve) along the anterior surface, and two circumferential paths (red curves) with one around the upper neck and another one around the lower neck. For the longitudinal path, the axial position went on the mid section from the upper neck to the lower neck; and for the circumferential paths, the angle started at the mid section of the anterior surface with the normal vector +k.

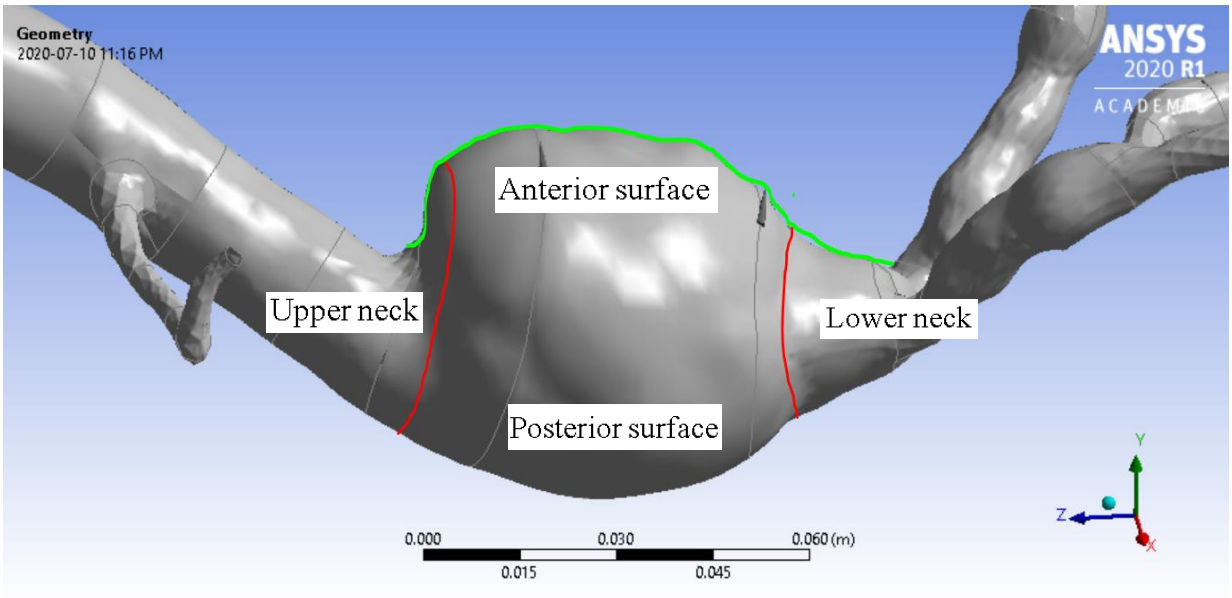

Figure 22 Illustration of the paths used for stress distribution plots

All the three graphs below showed that the stress variations follow the similar pattern for both scenarios, at rest and during exercise. The difference in stress values between both scenarios stayed relatively close in low stress regions. However, large differences were observed in high stress regions where the wall stresses during exercise were twice higher than the ones at rest.

Although the stress distributions seemed to be complex along all the paths, we could still find some remarkable behaviours. Along the anterior surface, we observed that high stress

regions were located at both necks and in the middle of the aneurysm. At the upper neck, high stresses occurred when the angle was close to 0°, whereas the peak stresses occurred at $\pm$ 60° at the lower neck.

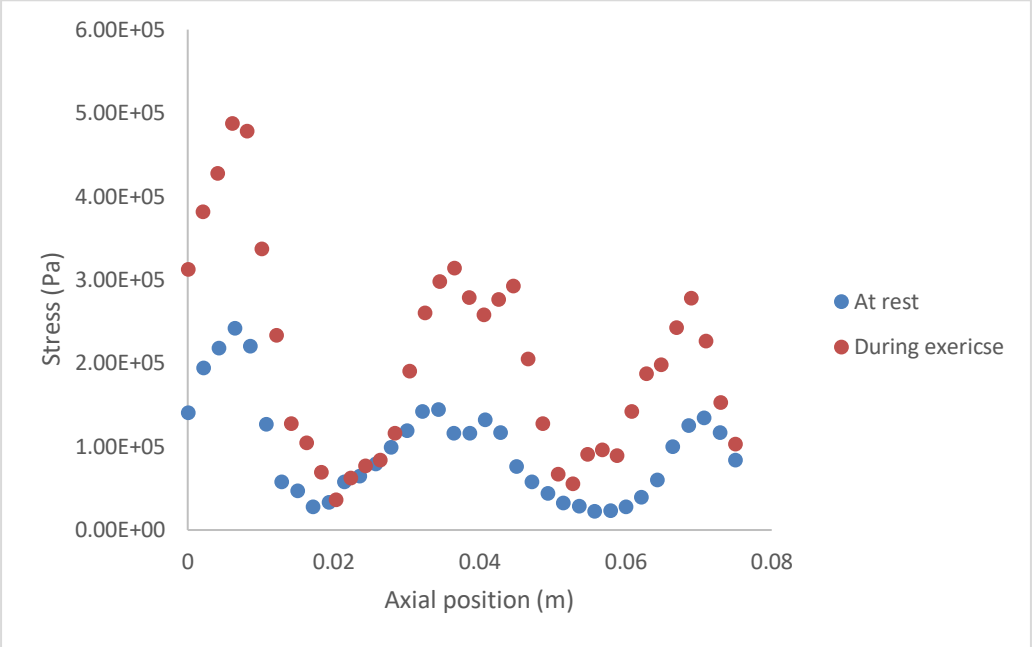

Figure 23 Stress distribution at mid-section

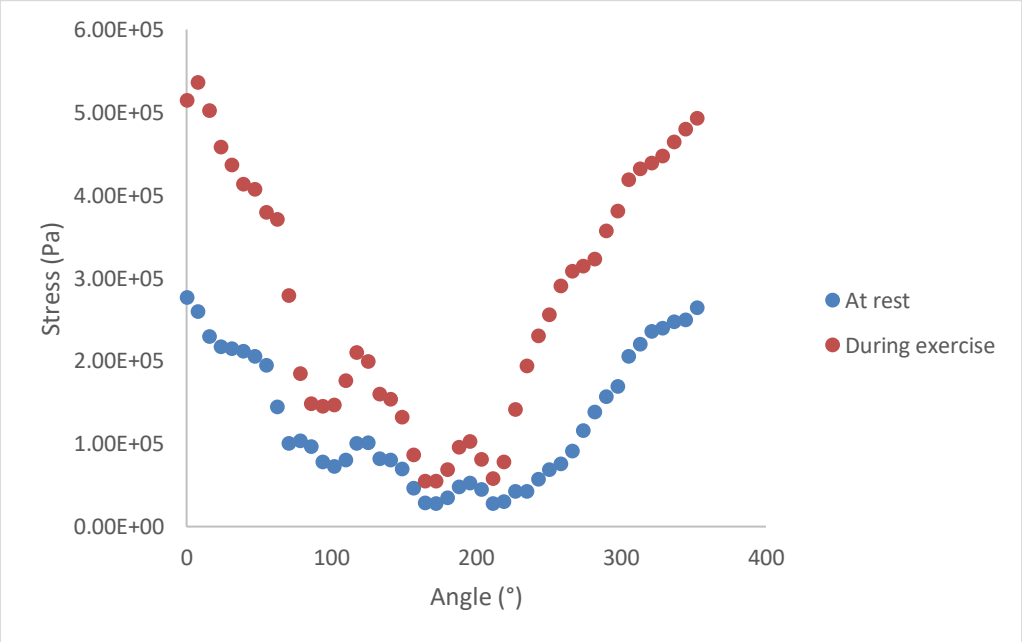

Figure 24 Stress distribution at upper neck

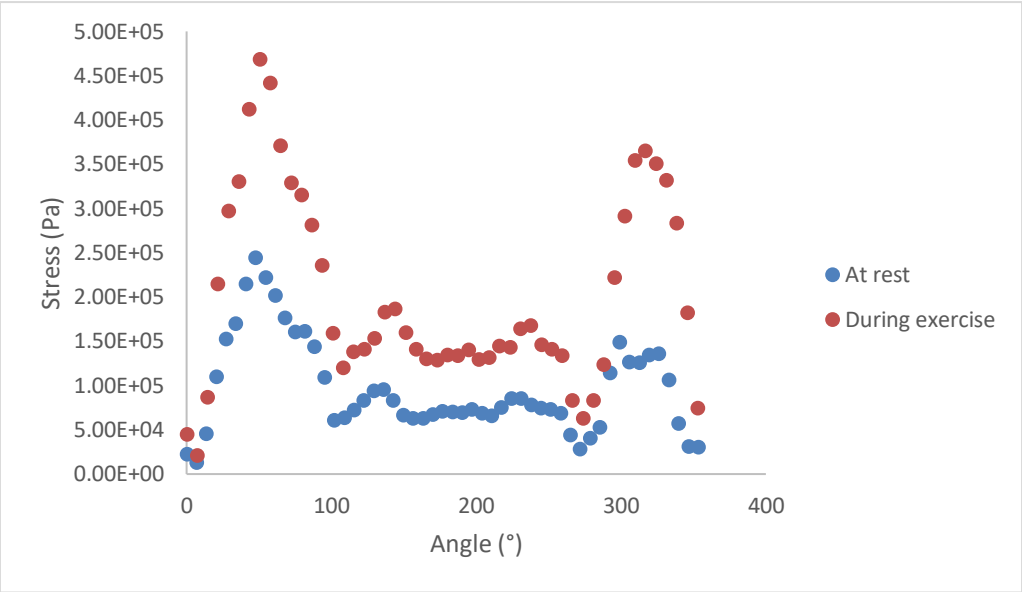

Figure 25 Stress distribution at lower neck

3.3 Viscoelastic Behaviour

The purely elastic model and viscoelastic model were simulated in both cases to study the impact of viscoelasticity on the wall stress. The maximum stress level was closely related to the pressure load, and it was much higher with the patient undergoing an exercise due to a high systolic pressure. In both cases, the purely elastic model showed a higher stress level than the viscoelastic model for a give strain. With time following the viscoelastic curve clockwise, this difference increased as time went by. Meanwhile, the prediction of the peak stress at the end of systole stayed very close for both models in both scenarios. As viscoelastic properties were introduced, the aortic wall appeared to have a larger deformation, shifting the peak stress at a larger strain level. The residual strain of approximately 0.05 was observed for the viscoelastic model, which reduced the stress concentration in the aorta under physiological load.

One major characteristic of a viscoelastic material is the presence of energy loss during a loading and unloading cycle. To evaluate the energy loss, curve fitting was used separately to the systole and diastole regions. During systole, the stress increased rapidly in an almost linear way

due to the rapid increase of the pressure load. During diastole, the stress decreased slowly, and a second order polynomial showed to be a better fit. Using the method presented in section 1.2, the energy loss was 15.5% for a heartbeat at rest, and 7.7% for a heartbeat during exercise. Clearly, the energy loss depended on the strain rate, and a higher strain rate would result in a more elastic behaviour of the material.

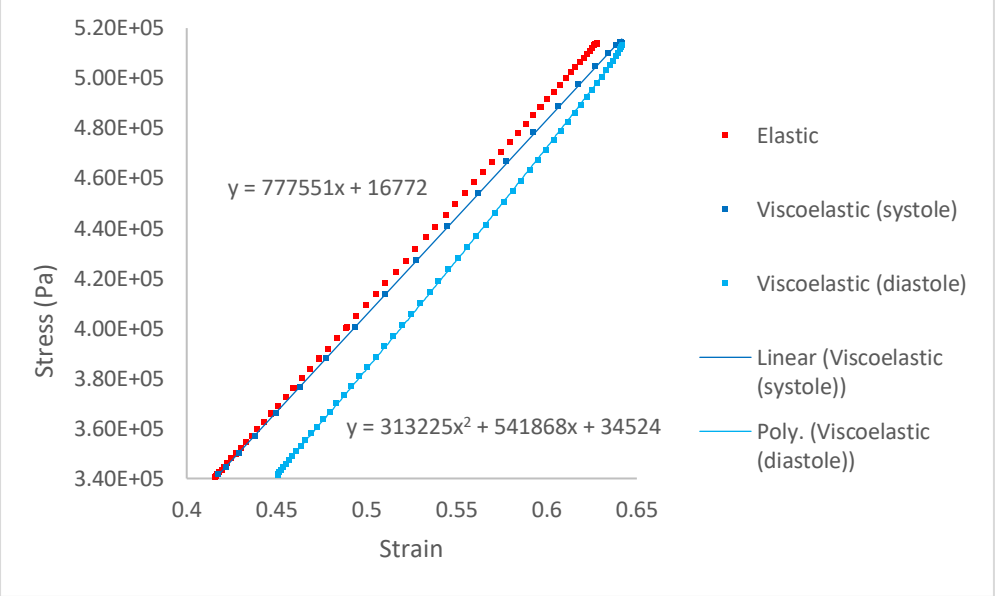

Figure 26 Stress-strain curve at the maximum wall stress location (at rest)

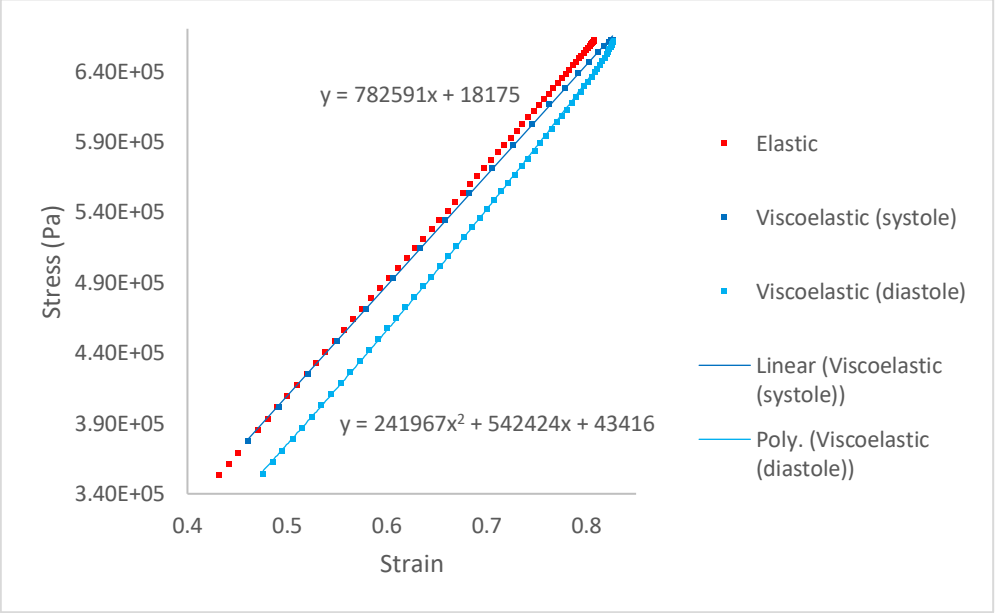

Figure 27 Stress-strain curve at the maximum wall stress location (during exercise)

3.4 Limitations of the Result

The model developed in this research did have some limitations to be kept in mind. In this study, we only considered one geometry. More patient specific geometries would be required to have a better understanding of the wall stress distribution of an AAA using viscoelastic model. With regard to the rationale, some assumptions were not based on reliable experimental evidence, but instead motivated by experimental limitations. The real arterial tissue was shown to be hyperelastic anisotropic [18]. However, the 10% PVA used in this research was an isotropic material. Thus, the result should not be taken as proof of similarity in mechanical behaviour between both circumferential and axial directions for AAA. In addition, the hyperelastic data was also missing in this research, and consequently the linear elastic properties were used as a reference of comparison in section 3.3. Finally, the aortic wall in general is not homogeneous along its thickness. In stead, it is composed of three layers: intima, media and adventitia with a significant difference of stiffness values. For the sake of model efficiency, one-layer model was used in this research with the average values of linear elastic properties. However, one must keep in mind that the stress in a three-layer wall was shown to be slightly higher than in a one-layer wall [6].

The wall stress estimation of an AAA is patient specific, since the aortic tissue in each patient has different elastic and viscous properties due to due to heart rate and blood pressure [19]. In terms of elastic properties, a loss of smooth muscle cells and increase in collagen content further increases the tissue stiffness [20]. This is particularly present among old patients. In terms of viscous properties, the energy loss is approximately 15% in a normal human aortic cell. As the AAA worsens and the aorta dilates, there is an exhibition of greater energy loss [21]. Due to the limitation of the samples, only one set of viscoelastic properties of a health cell was used in this

research. However, we need an adjustment of these properties to adapt specific patients and obtain more accurate results.

There were also many other factors that affected the accuracy of our computational stress analyses. In the geometry acquisition, 1 mm spacing between 2D images was a bit too large to capture all the details of the aneurysm. More errors were then added up during geometry parametrization and meshing because each step involved some approximation. In addition, due to the lack of information, regional variations in wall thickness were not considered either, which would lead to an overestimation of stress if the average thickness used was thicker than the actual wall thickness, and an underestimation of stress if it was thinner than the actual wall thickness [22]. Finally, the pressure profiles used in this research were only an approximation, and more realistic profiles would be required to render a more realistic model.

4. Conclusion and Future Work

4.1 Conclusion

In this research, a new model for AAA was developed using viscoelastic properties of the aortic cell. The geometry of the AAA was obtained from medical imaging techniques and parametrized with the reverse engineering tools in Ansys Mechanical. The viscoelastic properties were acquired from the experimental data of 10% PVA and modelled with Prony shear series. Two different pressure profiles were used in this paper, at rest and during exercise, and one cardiac cycle was simulated in both scenarios.

It was shown that the stress contour was very complex, and the maximum displacement did not correspond to the maximum stress state. In all the cases, the maximum stress occurred at both necks of the aneurysm, and the peak stress was twice larger in the case of a cardiac cycle during the exercise. Finally, compared to the linear elastic model, the viscoelastic model resulted in a larger strain and a lower stress level for a given strain state, leading to a more accurate estimation. This work did present some limitations in the accuracy of result due to the lack of precision in the geometry and data acquisitions, and in the generality of the conclusions due to the lack of samples. However, some meaningful results were obtained to encourage more research to be oriented into this direction.

4.2 Future Work

Some future work is encouraged to address the limitations of this research. One direction of the work is to collect more geometry samples to study the generality of the conclusions in this paper. A more sophisticated model is also required in obtaining a better estimation of the wall

stress. We highly encourage the researchers to use actual aortic cells in the evaluation of the mechanical properties so that the anisotropy and hyperelasticity can be considered. In addition, a three-layer model would also be preferred to render a more realistic model. Finally, one can use Fluid-Structure interaction (FSI) model to take the effect of fluid dynamics into account in order to obtain a more realistic pressure profile and better evaluation of aortic wall stress.

References

[1] M.L. Raghavan, and David A. Vorp, "Toward a biomechanical tool to evaluate rupture potential of abdominal aortic aneurysm: identification of a finite strain constitutive model and evaluation of its applicability," *Journal of Biomechanics*, 33(4):475-482, 2000.

[2] A. N. Azadani, S. Chitsaz, A. Mannion, B. A. Mookhoek, A. Wisneski, J. M. Guccione, M. D. Hope, L. Ge, and E. E. Tseng, "Biomechanical Properties of Human Ascending Thoracic Aortic Aneurysms," *The Annals of Thoracic Surgery*, 96(1):50-8., 2013.

[3] G.G. Belz, "Elastic properties and Windkessel function of the human aorta," *Cardiovascular Drugs and Therapy*, vol. 9, pp.73–83, 1995.

[4] Z. Wang, M. J. Golob, and N. C. Chesler, "Viscoelastic Properties of Cardiovascular Tissues," *Viscoelastic and Viscoplastic Materials*, chap. 7, 2016.

[5] D.A. McDonald, "The elastic properties of the artery wall," *Blood Flow in Arteries*, pp. 238-282, 1974.

[6] F. Gao, Z. Guo, M. Sakamoto, and T. Matsuzawa, "Fluid-structure Interaction within a Layered Aortic Arch Model," *Journal of Biological Physics*, 32:435–454, 2006

[7] D. Zhang, D. Arola, and C. D. Eggleton, "Measurement of Poisson's ratio of bovine aorta using Digital Image Correlation," *24th Annual Conference and the Annual Fall Meeting of the Biomedical Engineering Society*, Houston, TX, 10.1109/IEMBS.2002.1106385, 2003

[8] L. E. Millon, C. J. Oates, and W. Wan, "Compression Properties of Polyvinyl Alcohol – Bacterial Cellulose Nanocomposite," *Wiley InterScience*, London, ON, DOI: 10.1002/jbm.b. 31364, 2009

[9] T. Friedman, M. Michalski, T. R. Goodman, and J. E. Brown, "3D printing from diagnostic

images: a radiologist's primer with an emphasis on musculoskeletal imaging—putting the 3D printing of pathology into the hands of every physician," *Skeletal Radiology,* 45(3), 307-321. doi:10.1007/s00256-015-2282-6, 2016

[10] J. Garcia, "Patient specific surgical simulation of the ascending thoracic aorta,", *A thesis submitted to McGill University in partial fulfillment of the requirements for the degree of Doctor of Philosophy in Mechanical Engineering,* pp. 50-60, 2019

[11] D. Bommes, B. Lévy, N. Pietroni, E. Puppo, C. Silva, and M. Tarini, D. Zorin, "State of the Art in Quad Meshing," *COMPUTER GRAPHICS Forum,* Volume xx, Number z, pp. 1–24, 2012.

[12] J. F. Shepherd, and C. R. JOHNSON, "Hexahedral mesh generation constraints," *Engineering with Computers 24,* vol. 3, pp. 195–213, 2015.

[13] T. Avraham, "Mesh Quality," *Knowing the Mesh,* Part I, 2019 [Online]. Available: https://allaboutcfd-tomersblog.com/

[14] J. Lantz, J. Renner, and M. Karlsson, "Wall shear stress in a subject specific human aorta — influence of fluid-structure interaction," *International Journal of Applied Mechanics,* vol. 3, no. 4, pp. 759-778, 2011.

[15] R. P. Mazzoccante, I. R. Castro de Sousa, R. M. Dos Santos Pereira, T. F. de Lima Souza, J. F. Vila Nova de Moraes, and C. S. G. Campbell, "Effects of the alternance between aerobic and resistance exercise in different concurrent exercise sessions on blood pressure responses of healthy adults: a controlled and randomized study," *Rev Bras Educ Fís Esporte,* 30(2):245-53, 2016.

[16] M.L. Raghavan, and D. A. Vorp, "Toward a biomechanical tool to evaluate rupture potential of abdominal aortic aneurysm: identification of a finite strain constitutive model and evaluation of its applicability," *Journal of Biomechanics,* 33:475-482, 2000.

[17] H. C. Han, and Y. C. Fung, "Direct Measurement of Transverse Residual Strains in Aorta,"

The American Journal of Physiology, 270(2 Pt 2):H750-9, doi: 10.1152/ajpheart.1996.270.2.H750., 1996.

[18] T.E. Carew, R.N. Vaishnav, and D.J. Patel, "Compressibility of the arterial wall," *Circulation Research 23,* pp. 61-68, 1968.

[19] T. Länne, B.Sonesson, D. Bergqvist, H. Bengtsson, and D. Gustafsson, "Diameter and compliance in the male human abdominal aorta: influence of age and aortic aneurysm," *European journal of vascular surgery,* 6(2), 178-184, 1999.

[20] A. Emmott, J. Garcia, J. Chung, K. Lachapelle, I. El-Hamamsy, R. Mongrain, and R. L. Leask, "Biomechanics of the ascending thoracic aorta: A clinical perspective on engineering data," *Canadian journal of cardiology,* 32(1), 35-47, 2016.

[21] J. Chung, K. Lachapelle, E. Wener, R. Cartier, B. De Varennes, R. Fraser, and R. L. Leask, "Energy loss, a novel biomechanical parameter, correlates with aortic aneurysm size and and histopathologic findings," *The Journal of Thoracic and Cardiovascular Surgery,* vol. 148, pp. 1082-1089, 2014.

[22] J. Shum, G. Martufi, E. Di Martino, C. B. Washington, J. Grisafi, S. C. Muluk, and E. A. Finol, "Quantitative Assessment of Abdominal Aortic Aneurysm Geometry," *Annals of Biomedical Engineering,* 39(1):277-86, 2011.